The p73 DNA Binding Domain Displays Enhanced Stability Relative to Its Homologue, the Tumor Suppressor p53, and Exhibits Cooperative DNA Binding[†]

Seema Patel,[‡,§] Tam T.T. Bui,[§] Alex F. Drake,[§] Franca Fraternali,[‡,⊥] and Penka V. Nikolova*[,‡,§]

Department of Biochemistry and Pharamceutical Sciences Research Division, School of Biomedical & Health Sciences, King's College London, 150 Stamford Street, London SE1 9NH, United Kingdom, and Randall Division of Cell and Molecular Biophysics, New Hunt's House, Guy's Campus, King's College London, London SE1 1UL, United Kingdom

Received November 23, 2007; Revised Manuscript Received January 14, 2008

ABSTRACT: The p53 protein family is involved in the control of an intricate network of genes implicated in cell cycle, through to germ line integrity and development. Although the role of p53 is well-established, the intrinsic nature of its homologue p73 has yet to be fully elucidated. Here, the biochemical characterization and homology-based modeling of the p73 protein is presented and the implications for its function(s) examined. The DNA binding domains (DBDs) of p53, p63, and p73 bind to the specific target site of a 30-mer *gadd45* dsDNA, as tested by EMSA. The monomeric DBDs bind cooperatively forming tetrameric complexes. However, a larger construct consisting of p73 DBD plus TET domain (p73 CT) and the corresponding p53 DBD plus TET domain (p53 CT) bind *gadd45* differently than the respective DBDs. Significantly, p73 DBD exhibited enhanced thermodynamic stability relative to the p53 DBD but not compared to p63 DBD as shown by DSC, CD, and equilibrium unfolding. The p73 CT is less stable than p73 DBD. The modeling data show distinct electrostatic surfaces of p73 and p53 dimers when bound to DNA. Specifically, the p73 surface is less complementary for DNA binding, which may account for the differences in affinity and specificity for p53 REs. These stability and DNA binding data for p73 in vitro enhance and complement our understanding of the role of the p73 protein in vivo and could be exploited in designing strategies for cancer therapy in places where p53 is mutated.

The tumor suppressor protein p53 is known to be at the center of a complex regulatory network exhibiting diverse and global functions ranging from coordinating DNA repair, cell-cycle arrest, and apoptosis, through to regulation of mitochondrial respiration, glucose metabolism, and autophagy in order to protect the genomic integrity and prevent cancer (*1*). Nevertheless, how p53's function is affected by the newly identified p53 isoforms or the presence of isoforms of its homologues p73 and p63 remains to be elucidated (*2*). The key functional domains of the p53 protein, a transactivation domain (TA)[1], a DNA-binding domain (DBD) and a tetramerization domain (TET), are shared also by the homologues, p73 and p63 (*3, 4*). Both p63 and p73, but not p53, have a C-terminal extension (sterile alpha motif, SAM, domain), that has been suggested to be involved in protein–protein interactions with as yet unidentified signaling and/or regulatory proteins (*5, 6*). Although p53, p63, and p73 are similar in their ability to induce transcription, cell-cycle arrest, and apoptosis, each of them appears to play a distinct role in development and tumor suppression (*7–9*). Significantly, mutations in p73 and p63 in tumors are extremely rare despite the high sequence homology (62 and 58%, respectively) with p53 in the highly conserved DNA-binding domain, where the vast majority of p53 cancer-associated mutations are found (*10*). Like p53, p73 is expressed at very low levels in normal human tissues. In contrast to p53, the most common cancer-specific alteration is an overexpression of p73 rather than a loss of expression. The cause of p73 (and p63) overexpression, as well as the pathways leading to their activation, is not well understood. p63 and p73 can mimic p53, but also counteract the functions of p53 (*11*). Interestingly, it has been reported that the transcription factor E2F-1 can induce p53-independent apoptosis and that one mechanism appears to involve p73 (*12, 13*). A fundamental question that requires further investigation is to establish the extent to which p73 and p63 share a role with p53 in tumor suppression (*9, 14–16*). The data on the possible mechanisms of p73 and p63 involvement in tumor suppression have been controversial due to the fact that the dependence of p53 on p73 and p63 for apoptosis is tissue specific (*15*). It has been reported that like p53, p73 is likely to bind DNA as a tetramer, whereas the various p73 isoforms can form

[†] This work was supported by the Association of International Cancer Research (AICR), The University of London Central Research Fund, and The Royal Society Research Grants.

* To whom correspondence should be addressed. Address: King's College London, School of Biomedical and Health Sciences, Deptartment of Biochemistry & Pharmaceutical Science Research Division, Franklin-Wilkins Building, 150 Stamford Street, London SE1 9NH, U.K. Phone: 44(0) 207-848-4276. Fax: 44(0) 207-848-4500. E-mail: penka.nikolova@kcl.ac.uk.

[‡] Department of Biochemistry, School of Biomedical and Health Sciences, King's College London.

[§] Pharmaceutical Sciences Research Division, King's College London.

[⊥] Randall Division of Cell and Molecular Biophysics, King's College London.

[1] Abbreviations: TA, transactivation domain; DBD, DNA binding domain; CT, DBD plus tetramerization domain; TET, tetramerization domain; EMSA, electrophoretic mobility shift assay; DSC, differential scanning calorimetry; CD, circular dichroism; AGF, analytical gel filtration, p53 RE, p53 response element.

10.1021/bi7023207 CCC: $40.75
Published on Web 02/09/2008

hetero-oligomers (*8, 17*). Furthermore, it was shown that p73 does not require its extreme C-terminal domain for apoptosis and truncation of the latter did not affect the DNA binding of p73 (*8*). Because the components of the biological network that controls the p53 pathway have begun to emerge, it should now be possible to address precise questions regarding the molecular mechanisms that regulate this complex network. Wang et al. have recently reported the discovery of small-molecule modulators targeting p73, which may be exploited for tumor suppression, in cases where p53 is absent, or in the presence of mutant p53 (*18*).

The work presented here is focused on the biochemical characterization and homology-based modeling of the p73 protein in order to shed light that can help to understand the function of p73 at a molecular level. Specifically, the stability and DNA binding behavior of p73 is compared to the two homologous proteins p53 and p63, and the functional implications examined. The thermodynamic properties of p73 were assessed by chemically induced equilibrium denaturation, which was measured by fluorescence spectroscopy. To investigate the affinity of p73 for dsDNA, we used band shift assays. In addition to the chemical equilibrium urea denaturation, thermal stability was monitored by differential scanning calorimetry (DSC) and circular dichroism (CD) spectroscopy. To gain further insight into the p73 protein and its DNA interactions, structure-based molecular modeling was carried out for p73 DBD based on the p53 X-ray structure in complex with DNA using the PDB accession number 2aco (*19*).

MATERIALS AND METHODS

Gene Cloning, Mutagenesis, Protein Expression, and Protein Purification. The cloning, expression and purification of human p53 DBD encoding amino acid residues 94–312 were performed as described in Bullock et al. (*20*). The cloning of p73 DBD encoding residues (104–333) using *Bam*HI-*Eco*RI cloning sites and of p73 CT encoding residues (104–383) using NdeI-*Eco*RI cloning sites were performed using pRSETA (Invitrogen) expression vector without the His tags. The proteins were expressed in *Escherichia coli* strain *BL21 (DE3)* or its derivative *C41 (DE3)* cells (Avidis), which can give higher yields of soluble protein (*21*). Cell cultures were grown in 2xTY media containing ampicillin at 37 °C to $A_{600} = 0.8$ and the temperature reduced to 22 °C before overnight induction with 1 mM IPTG (isopropyl β-D-thiogalactoside). Cells were harvested at 4 °C by centrifugation and lysed in either 50 mM Tris-HCl or sodium phosphate buffer, pH 7.2, 5 mM DTT supplemented with complete EDTA-free protease inhibitor cocktail (Roche) using Bug Buster Protein Extraction Reagent plus Benzonase Nuclease (Novagen). The resulting soluble fraction was loaded onto a SP Sepharose cation exchange column (GE Healthcare) and eluted with a NaCl gradient. The next purification step involved affinity chromatography by a HiTrap Heparin Sepharose column (GE Healthcare). Gel filtration chromatography was applied using Superdex 75 or 200 columns (GE Healthcare) and 50 mM sodium phosphate pH 7.2, 5 mM DTT, 150 mM NaCl. Columns were kept at 4 °C using a cooling water jacket. Protein concentrations were determined spectrophotometrically by the method of Gill and von Hippel (*22*). The purified proteins were frozen in small aliquots in liquid nitrogen and stored at −80 °C. The molecular masses of the proteins were confirmed by electrospray mass spectrometry based upon the theoretical molecular weight, p73 DBD = 25655 and p73 CT = 31378. The full-length p73 protein (alpha) has 636 amino acids and MW = 69623. The extinction coefficients, ϵ_{280}, were calculated to be 16 770, 19 330, and 52 425 $M^{-1}cm^{-1}$, respectively. Constructs were verified by sequencing using universal T7 and T7TERM primers. The protein fractions were purified to homogeneity as assessed by SDS-PAGE (gels not shown). The protein constructs for p63 DBD (154–365), p53 DBD (94–312), and p53 CT (94–360) were purified using the methods outlined above.

Analytical Gel Filtration (AGF). Analytical gel filtration was performed at 20 ± 1 °C in 50 mM sodium phosphate, pH 7.2, 200 mM NaCl, 5 mM DTT using a Superdex 200 10/300 column (GE Healthcare). The proteins were injected at a concentration of 40 μM with an injection volume of 100 μL and the milli-absorbance units (mAu) at 280 nm were recorded. Standard molecular weight markers (GE Healthcare) were used to calibrate the column. A calibration curve was generated with the K_{av} vs log molecular weight according to the manufacturer's instructions. From this curve, the molecular weight of the proteins of interest was determined.

Circular Dichroism Spectroscopy (CD). CD measurements were performed in 10 mM sodium phosphate, pH 7.2, 150 mM NaCl, and 4 mM DTE using the Applied Photophysics Chirascan spectrometer. The protein concentrations were 0.2 mg/ml. Far-UV spectra were recorded in the region 260–180 nm, using a 0.5 mm cell path length. The following parameters were employed: spectral bandwidth 1 nm, step size 0.5 nm and time-per-point 3.0 s. Temperature was controlled by a Melcor peltier temperature controller. For the melting curves, the Melcor unit was set to change temperature from 4 to 98 °C at a rate of 2 °C/min with a 2 °C step size, and a 0.2 °C tolerance. A 10 s time-per-point CD measurement time was used. The temperature was measured directly with a thermocouple probe in the protein solution. All spectra were buffer baseline corrected. Protein secondary structure contents were assessed using a principal component regression method (*23*).

Chemical Equilibrium Denaturation. Chemical equilibrium-mediated denaturation studies were performed as described previously (*24, 25*). Briefly, the free energy of unfolding was determined at 10 °C by urea-induced equilibrium denaturation experiments by monitoring the intrinsic fluorescence intensity. All samples were prepared using a Hamilton Microlab dispenser. The final protein concentration used was 2 μM. Sodium phosphate buffer at pH 7.2, 5 mM DTT was used and the measurements performed either on an Aminco-Bowman series 2 or Perkin-Elmer LS50 fluorimeter. The intrinsic fluorescence spectra, using $l_{ex} = 280$ nm, were recorded between 300 and 360 nm. For each experimental data point on the denaturation curve, 100 μL of 18 μM protein were added to 800 μL of the corresponding denaturant solution. Samples were incubated at constant temperature (10 °C) overnight and measured in a 1 mL quartz cuvette. The free energy of unfolding in the presence of the denaturant was determined based on the following equations:

$$\Delta G = \Delta G(H_2 0) - m[D] \quad (1)$$

$$[D]_{50\%} = \Delta G(H_2 0)/m \quad (2)$$

Table 1: Thermodynamic Parameters of the p53 Family of Proteins[a]

proteins	m[b] (kcal mol^{-1}M^{-1})	$[D]_{50\%}$[c] (M)	ΔG (H_20)[d] (kcal mol^{-1})	T_m (°C) DSC	T_m (°C) CD
p53 DBD	2.40 ± 0.12	3.20 ± 0.01	7.86	42.0[e]	42.0
p63 DBD	2.20 ± 0.30	5.33 ± 0.12	11.72	60.1[f]	59.0
p73 DBD	2.63 ± 0.10	3.98 ± 0.01	10.46	51.2	49.5
p73 CT	2.11 ± 0.30	3.80 ± 0.05	8.02	47.4	47.0

[a] Data presented for urea-induced equilibrium unfolding for p53 DBD, p63 DBD, p73 DBD, and p73 CT were collected at 10 °C in 50 mM sodium phosphate, 5 mM DTT, pH 7.2, and 2 μM protein concentrations. The data were analyzed as described in the Materials and Methods section. The apparent melting temperatures obtained by DSC and CD for all proteins were presented in degrees centigrade. The experimental conditions for the DSC and CD are described in the material and methods section. [b] m (kcal mol^{-1} M^{-1}) is a constant proportional to the increase in solvent accessible surface area between the native and the denatured state of the proteins (*41*). The m value of 2.4 for the p53 DBD is that for the wild-type p53 DBD and not the average of mutants and wild-type p53 DBD, calculated to be 2.7. This is to reflect the more accurate comparison between the wild-type of all constructs involved. [c] $[D]_{50\%}$ (M) is the denaturant concentration at which half of the protein is denatured. [d] ΔG (H_20) (kcal mol^{-1} M^{-1}) is the free energy of unfolding in water, according to eqs (*1*) and (*2*) in the Materials and Methods section. [e] DSC data for the apparent T_m of wild-type p53 DBD as measured and reported previously (*39*). [f] DSC data for the apparent T_m of p63 DBD as reported in Klein et al. (*38*).

where ΔG is the free energy of unfolding, ΔG (H_20) is the free energy of unfolding in the absence of denaturant, [D] is the denaturant concentration, $[D]_{50\%}$ is the denaturant concentration at the midpoint of the transition, and m is the constant of proportionality that is related to the solvent-accessible surface area between the native and the denatured state of the protein (*26*). The experimental data were fitted to a two-state transition curve with the fluorescence of the folded and unfolded states dependent on the denaturant concentration. Nonlinear least-squares analyses in the KALEIDAGRAPH program were employed to give the values of the linear slope of the transition from native to denatured state, $[D]_{50\%}$, m, and the corresponding standard errors.

Electrophoretic Mobility Shift Assays (EMSA). The sequence-specific DNA-binding of p73 was determined and compared to that of p53 by performing bandshift assays (gel retardation or electrophoretic mobility shift assay) using 0.7% agarose gels. The binding affinity of p73 to DNA was investigated by selecting a double-stranded 30-mer of *gadd45* as a model system. The dsDNAs were annealed from HPLC-purified single-stranded oligonucleotides (Sigma Genosys). The binding sequence for *gadd45* was that published by Jayaraman et al., (GAGCAGAACATGTCTAAGCATGCTGGGGCTC) (*27*). The oligonucleotides were annealed in 10 mM Tris, 100 mM NaCl at 99 °C for 5 min and slowly cooled. The dsDNA was purified on a Mono Q HR 10/10 column using buffer A (10 mM Tris pH 8.0, 20% ethanol) and buffer B (10 mM Tris, pH 8.0, 20% ethanol, 1 M NaCl). The DNA concentration was measured spectrophotometrically at 260 nm. The gels were run in TB (Tris-borate) buffer (90 mM Tris base, 90 mM boric acid, pH 8.3), with a constant current (30 mA). Protein−DNA complexes were supplemented with 0.1 vol. of 20% (v/v) glycerol, 0.1% (w/v) bromophenol blue. Samples were incubated for 30 min at 20 °C prior to loading onto the gels. The DNA concentration was kept constant at 1×10^{-5} M, whereas the protein concentration was varied from 0.5 to 8×10^{-5} M. After the gel electrophoresis, the gels were incubated under gentle stirring in water supplemented with ethidium bromide for about 1 h before examination under UV light. For the native gel, the DNA concentration was kept constant at 15 μM with increasing concentrations of p53 and p73 DBD titrated to give 1:1, 1:2, 1:3, and 1:4 ratios. Complexes were incubated at 4 °C and supplemented with native PAGE 4× sample buffer prior to loading on the gel. The prepoured 4–16% native PAGE (Invitrogen) gels were run at 150 V at 4 °C constant for ~2 h and stained with Coomassie Blue for protein visualization.

Differential Scanning Calorimetry (DSC). DSC studies were performed using a Microcal VP-DSC microcalorimeter (Microcal, Amherst, MA). The data were analyzed using the ORIGIN software (Origin Laboratory Corporation) giving the apparent melting temperatures (T_m). The scans for p73 DBD and p73 CT were recorded using a scan rate of 1 °C per min and were dialyzed prior to use in 50 mM sodium phosphate, 5 mM DTT, pH 7.2, and degassed under vacuum using argon. All proteins were filtered through 0.1 mm Acrodisc filter (Whatman). Temperature scans were collected from 5 to 90 °C. Dialysis buffer was used for baseline scans.

Modeling. The model structure of p73 was obtained by homology modeling from the crystal structure of p53 (PDB accession number 2aco) (*19*), with which it shares about 60% sequence identity. It is well-known that a sequence identity threshold for obtaining a reasonable model is 30% (*28*). Sequence alignments were generated by using the T-coffee method (*29*). 3D models were generated using the MODELER package, which can generate a large number of models and performs an optimization of the generated models with respect to a defined objective function. This software has been used for wide-scale structure modeling of genomes (*30*). The selected models were chosen on the basis of the objective function's score. To refine the models, energy minimizations were performed with the GROMACS package (*31*) using the GROMOS96 force field (*32*). GROMACS package and self-written programs have been used for the analysis of the data. Images were produced with visual molecular dynamics (VMD) 1.8.5 (*33*). The dimer of p73 was constructed by analogy to the dimer of p53 in the 2aco coordinate file (chains B and C). To characterize the interaction surface, the program POPS comp was used (*34, 35*) to detect the residues that are buried upon dimerization (Table 2). POPScomp calculates the solvent accessible surface area (SASA, in Å^2) of each residue before and after the formation of the dimer. The structural alignment was performed with the program aliss (Jens Kleinjung, personal communication). Electrostatic surfaces were calculated by the use of the program PYMOL (*36*) with the implemented subroutine surface APBS (*37*).

RESULTS

Protein Purification. To understand whether differences in protein stability and DNA binding affinity can help explain the differences in biological functions between p53, p63, and

Table 2: Buried Solvent Accessible Surface Areas for p73 DBD and p53 DBD upon Dimerization[a]

residue	phobic (%)	philic (%)	total (%)
	(A) p53 DBD Chain C		
CYS 176	1.3	0.0	1.3
PRO 177	41.6	1.2	42.8
HIS 178*	43.8	20.7	64.5
HIS 179	4.2	3.2	7.4
ARG 181	14.7	30.5	45.2
CYS 242	2.8	0.1	2.9
MET 243*	128.8	4.7	133.4
GLY 244	11.7	3.7	15.4
	(B) p53 DBD 180° Rotated Chain D		
CYS 176	1.4	0.0	1.4
PRO 177	**46.9**	**1.2**	**48.0**
HIS 178*	**43.5**	**20.9**	**64.4**
HIS 179	4.7	3.5	8.2
ARG 181	15.1	29.8	44.9
CYS 242	2.2	0.1	2.3
MET 243*	**127.7**	**4.7**	**132.3**
GLY 244	11.1	3.4	14.5
	(C) p73 DBD Chain C		
CYS 194	2.5	0.1	2.6
PRO 195	60.8	1.7	62.4
ASN 196*	25.0	77.0	101.9
HIS 197	0.9	0.4	1.3
GLU 198*	0.0	0.5	0.5
LEU 199*	11.6	0.0	11.6
CYS 262	0.2	0.0	0.2
VAL 263*	29.1	4.5	33.6
GLY 264	7.6	3.6	11.3
GLY 265*	0.2	0.3	0.5
	(D) p73 DBD 180° Rotated Chain D		
CYS 194	2.5	0.2	2.7
PRO 195	61.6	1.8	63.3
ASN 196*	25.0	76.7	101.8
HIS 197	1.0	0.3	1.4
GLU 198*	0.0	0.5	0.5
LEU 199*	13.7	0.0	13.7
CYS 262	0.2	0.0	0.2
VAL 263*	24.5	4.1	28.5
GLY 264	7.3	3.6	10.9
GLY 265*	0.1	0.3	0.4

[a] Surface areas are reported in angstroms. The most significant differences between p53 and p73 residues at the interface are highlighted in bold. Asterisks (*) indicate the residues that differ in the two structures upon DNA binding (see sequence alignment).

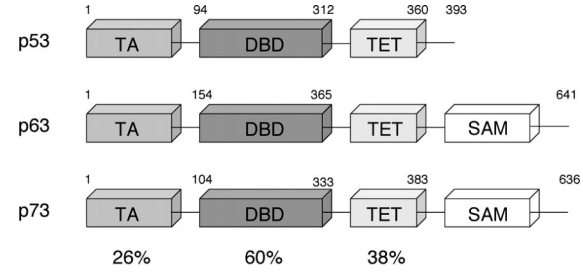

FIGURE 1: Schematic diagram of the domain structure organization of the p53 family of proteins. Domains common to all three proteins, namely, p53, p63, and p73, include the transactivation domain (TA), DNA-binding domain (DBD), and tetramerization domain (TET). The sterile alpha motif (SAM) is present in p73 and p63 but not in p53. Amino acid sequence identity between the proteins is indicated in percentage for the TA, DBD, and TET domains. The boundaries of the constructs used in this work are indicated for each protein.

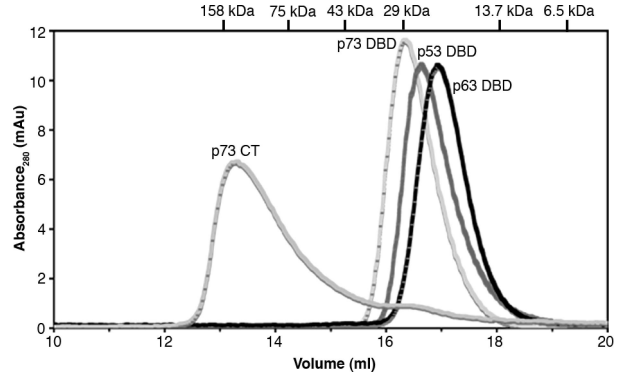

FIGURE 2: Analytical gel filtration chromatography profiles of p53 DBD, p63 DBD, p73 DBD, and p73 CT constructs. A Superdex 200 10/300 column was used with 50 mM sodium phosphate buffer, 5 mM DTT, 200 mM NaCl, pH 7.2, at flow rate 0.6 mL/min at 20 ± 1 °C. The retention volumes of proteins of known molecular mass (kDa) are indicated. Protein concentrations for the p53 family of proteins injected were 40 μM and the milli-absorbance units (mAu) at 280 nm were recorded. The injection volume was 100 μl. A calibration curve of K_{av} vs log molecular weight was created using standard molecular weight markers. By calculating the K_{av} value from the elution volume of each protein, the molecular weight of each protein was read from the extrapolated calibration curve. The molecular weights of p53 DBD, p63 DBD, p73 DBD, and p73 CT read from the curve were ~25, 22, 28, and 125, respectively, and correspond to the theoretical molecular weights of 24.5, 23.6, 25.5, and 125 (31.4 × 4), respectively. Note that the p73 CT elutes from the column as a tetramer.

p73, we cloned, expressed, and purified the proteins and carried out a biochemical characterization. The p73 DBD (104–333), p73 CT (104–383) and FL (full length) p73 alpha (1–636), shown in Figure 1, were cloned in pRSETA, expressed in *E. coli C41 (DE3)* and purified using a combination of cation-exchange, affinity. and size-exclusion chromatography. Similarly, p63 DBD (154–365) was cloned expressed and purified as described for p73 and p53 DBD (*24, 25*). The pRSETA vector was modified so that it does not carry the His tag. The boundaries of the constructs were based on comparisons with the p53 DBD (94–312), p53 CT (94–360), and FL p53 (1–393), as shown in Figure 1. The proteins were purified to homogeneity as judged by 12% SDS-PAGE and size-exclusion chromatography. The FL p73 protein expresses to a high degree but efforts to purify it from inclusion bodies resulted in extremely low yields of protein, which aggregated when subjected to refolding. The studies presented here are focused on the p73 DBD and p73 CT. The molecular masses of the proteins were confirmed by ES mass spectroscopy and size-exclusion chromatography (Figure 2).

The p53 protein family members differ significantly in stability - p73 DBD and p63 DBD are more stable than p53 DBD. The p73 CT is less stable than p73 DBD. The inherent stability and folding of the p73 protein was investigated and compared with that of the well characterized p53 and p63 homologues, using different spectroscopic methods, which provided complementary information.

(1) Fluorescence Spectroscopy. Intrinsic fluorescence spectroscopy is used as a probe of the tertiary conformation of the proteins under investigation. All the DBD's of the p53 family of proteins described here contain a single tryptophan. In the p73 and p63 members, this residue is conserved, whereas in p53 DBD, the tryptophan (located at position 146) is not conserved. The fluorescence spectra of both the native

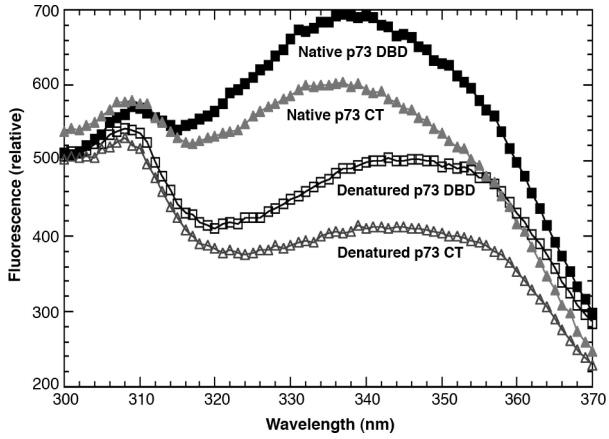

FIGURE 3: Fluorescence spectra of the native and denatured states of p73 DBD and p73 CT. The data were collected at 10 °C on Perkin-Elmer LS50 fluorimeter, using 2 μM protein concentration in 50 mM sodium phosphate buffer, 5 mM DTT, pH 7.2. Urea was used as denaturant. Excitation wavelength was 280 nm and the emission scans collected between 300 and 400 nm. The relative fluorescence intensity in absorbance units is indicated as a function of the wavelength (nm).

and urea-denatured p73 DBD and p73 CT are reported here for 2 μM protein concentrations. Native p73 DBD and p73 CT both show an emission $l_{max} \approx 338$ nm which shifts to $l_{max} \approx 346$ nm upon denaturation with urea (Figure 3). Similar results were reported for p53 DBD by Bullock et al., who interpreted this as a change for a partially buried tryptophan in the native state to an exposed tryptophan in the denatured state (*20*).

The emission wavelength shift, l_{em}, was used as a probe to monitor the thermodynamic stability of the proteins, using urea- and or guanidine hydrochloride-mediated equilibrium unfolding. The data for urea-mediated denaturation are presented in Table 1. These data indicate that the order of resistance to urea denaturation is p63 > p73 > p53, i.e., the p63 and p73 DBDs are more stable than p53 DBD.

(2) CD Spectroscopy. The protein folding states and the effects of temperature were evaluated by CD. The far-UV spectra of p53 DBD, p73 DBD, p63 DBD, and p73 CT are shown in Figure 4. All spectra were recorded at 4 and 20 °C prior to heating to 94 °C and cooling back to 4 °C. The CD spectra for p53 DBD and p63 DBD are in general agreement with the data previously published by Klein et al. (*38*). In solution, the core DNA binding domains of the p53 family of proteins would seem to contain mostly β-sheet structure, which is expected from the known crystal structure of p53 DBD (*4*). The CD secondary structure content analysis for p53 DBD spectra gives β-sheet = 38.8% and α-helix = 3.1% at 20 °C in solution at pH 7.2, in excellent agreement with the p53 data published by Bell et al., who reported β-sheet = 38.4% and α-helix = 8.4% (*39*). The corresponding calculations for p63 DBD gave β-sheet = 36% and α-helix = 13% at 20 °C, which is similar to that reported by Klein et al. (*38*). No CD data have been published on p73 DBD as yet, but the results here reveal that the conformation of the p73 DBD (β-sheet = 34.6% and α-helix = 7.4% at 20 °C) is similar to that of the p53 DBD and p63 DBD (*4, 38, 40*). However, when the spectra for the p73 DBD and p53 DBD were recorded at physiological temperature, the p73 DBD spectrum at 37 °C is virtually identical with the spectra recorded at 4 and 20 °C, whereas that of

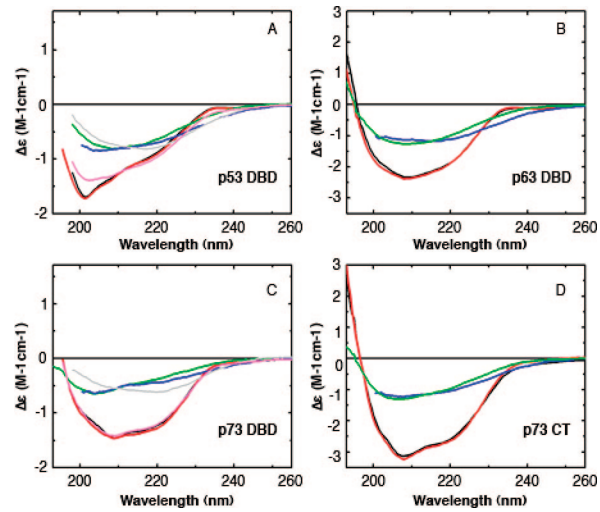

FIGURE 4: Far-UV CD spectra of (A) p53 DBD, (B) p63 DBD, (C) p73 DBD, and (D) p73 CT. The data in the region 260–180 nm were recorded on Chirascan spectrometer in 10 mM sodium phosphate, 150 mM NaCl, 4 mM DTE, pH 7.2, using 0.2 mg/ml protein concentrations and 0.5 mm cell path length. All spectra were buffer baseline corrected. Protein secondary structure contents were assessed using a principal component regression method (*23*). The data were converted to the differential molar circular dichroic extinction coefficient, $\Delta\epsilon$ (M^{-1} cm^{-1}). The CD spectra of the proteins were recorded at 20 °C (black), cooling to 4 °C (red), heated to 37 °C (pink), and then at the respective melting temperatures, T_m (grey), followed by heating at 95 °C (blue) and recooled to 20 °C (green).

p53 DBD is not and shows changes in the secondary structure, likely to be due to aggregation and or unfolding. Importantly, when the spectra for both p73 DBD and p53 DBD were recorded at their previously established apparent melting temperatures (T_m), namely, 42 °C for p53 DBD and 49.6 °C for p73 DBD, both proteins exhibited similar patterns of behavior, i.e., they showed spectra significantly different from the spectra recorded at lower temperatures, including that at 37 °C. This is also reflected in the changes in the secondary structures for both proteins.

Far-UV CD observations at physiological temperature for p73 DBD and p53 DBD are of particular importance. The data show that at physiological temperature, p73 DBD seems to be fully folded (Figure 4C). This observation is in sharp contrast with the data for p53 DBD at 37 °C (Figure 4A), which may have functional implications, especially in relation to the inability of some mutant p53 proteins to bind to DNA. Studies where p53 mutants have been shown to be unfolded, partially unfolded, and/or aggregated lack the ability to bind to DNA and have been well-documented (*20, 24, 41*).

Finally, the far-UV CD spectrum for the p73 CT domain shows a pronounced negative maximum at 208 nm consistent with a β-sheet = 31% and α-helix = 20.3% and that of a folded protein (Figure 4D).

(3) Enhanced Thermodynamic Stability of p73 Relative to p53 but Not p63 As Shown by DSC and CD. The DSC and CD data presented here concern apparent melting temperatures (T_m) because all protein constructs denatured irreversibly as a function of the temperature, certainly after heating to 94 °C (Figures 5 and 6). Similar results have been observed for full-length p53 (*40*), p53 DBD (*20*), and p63 DBD (*38, 39*). DSC measurements were carried out for p53 DBD, p63 DBD, p73 DBD, and p73 CT (Figure 5), yielding

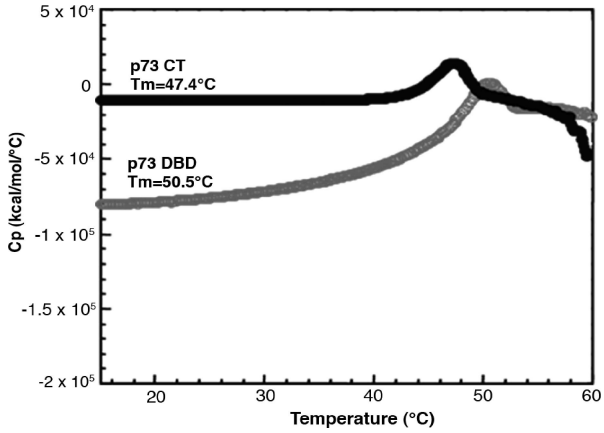

FIGURE 5: Thermal denaturation measurements by DSC for the p73 CT and p73 DBD. Data were collected on Microcal Microcalorimeter in 50 mM sodium phosphate, 5 mM DTT, pH 7.2, at 20 μM protein concentration. The apparent melting temperatures, T_m, are indicated. The heat capacity is shown as C_p.

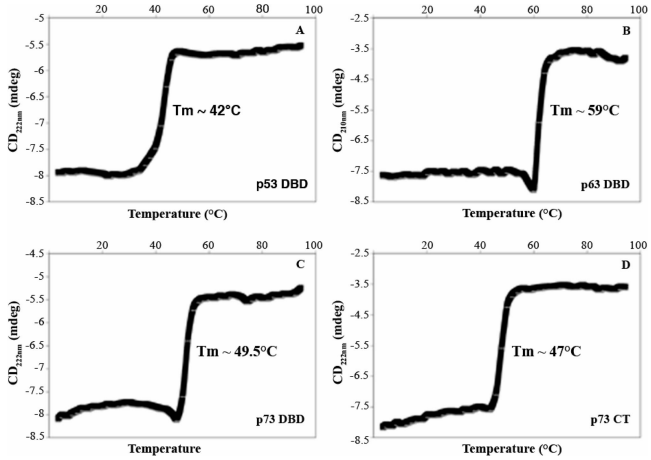

FIGURE 6: Thermal denaturation measurements by CD for the (A) p53 DBD, (B) p63 DBD, (C) p73 DBD, and (D) p73 CT. Except for p63 DBD (where 210 nm were used), the data were recorded at 222 nm on Chirascan spectrometer in 10 mM sodium phosphate, 150 mM NaCl, 4 mM DTE, pH 7.2, using 0.2 mg/ml protein concentrations and 0.5 mm cell path length. The apparent melting temperatures, T_m, are indicated.

the apparent melting temperatures listed in Table 1. The DSC measurements gave apparent T_m values similar to those observed previously for p53 DBD and p63 DBD (*20, 38, 39*). The apparent T_m values for p73 DBD and p73 CT are higher than those for p53 DBD and p53 CT (*20, 39*). The $T_m = 61$ °C for p63 DBD (*38*) is higher than the T_m of p53 DBD and p73 DBD.

The greater thermal stability of p63 and p73 relative to p53 observed by DSC was confirmed by the CD melting curves (Figure 6). The apparent melting temperatures obtained for each p53 family protein showed that p63 DBD is the most stable of the three with $T_m \approx 59$ °C (Figure 6B), followed by p73 DBD with $T_m \approx 49.5$ °C (Figure 6C) and then p53 DBD, which denatures with $T_m \approx 42$ °C (Figure 6A). The T_m for p53 DBD precisely matches that previously reported (*20*); the T_m of p63 DBD is within experimental error of the previously reported $T_m = 61$ °C (*38*). The T_m of p73 CT is ~47 °C (Figure 6D). It is worth noting that the p73 tetramerization domain alone has been described as being extremely stable, thermally reversible and does not start to unfold until at least 60 °C (*6*). It has been reported that the melting temperature of the p53 isolated tetramerization domain is between 72 and 75.2 °C (*39, 42, 43*). In the CD measurements, all the proteins showed irreversible temperature denaturation upon heating to 94 °C due to aggregation, and were unable to refold upon cooling to 20 °C. However, in the studies presented here, thermal denaturation is generally observed as a two-step process; this is not apparent in the DSC measurements. There is evidence in the CD thermal measurements of an unfolding step particularly in the p63 and p73 proteins prior to the main aggregation process. A "dip" can be observed in the CD thermal curves (see Figure 6) before the onset of the main transition. The apparent T_m values reported here refer to the aggregation step (Figure 6. and Table 1). The p53 protein is so thermally unstable that the two processes are not distinguished and only the aggregation step is observed. The concept of a two-step melting for the p53 family of proteins suggests that the thermally unfolded states of the isolated tetramerization domains do not aggregate. The data shown here demonstrate that the p63 and p73 proteins are more stable than p53.

DNA Binding Activity. Having established clear differences in the relative stabilities of the three homologous proteins it was of interest to investigate whether these differences might affect their DNA binding activity. The DNA binding activities of p73 DBD and p73 CT were analyzed and compared to those of p53 DBD and p63 DBD. In addition, p73 CT was compared to the corresponding p53 CT. *Gadd45* was used as a model promoter, which is known to bind all three homologous proteins. The p53 binding activity and specificity have been studied in great detail (*39, 41, 44*). Similarly, Klein et al. have published DNA binding data for p63 DBD with a limited set of p53 DNA binding promoters (*38*). However, p73 DNA binding specificity and selectivity so far have not yet been fully elucidated.

EMSA was used to test the DNA binding activity of p73 constructs to make comparisons with the binding activities of p53 and p63 (Figure 7A−D). p73 CT exhibited binding with all the 30-mer dsDNAs tested, namely *gadd45*, *mdm2*, *bax*, *Puma*, and *14–3–3* (only EMSA data for *gadd45* are shown in Figure 7D). For comparison, band shift EMSA was carried out with isolated p53 DBD, p63 DBD, p53 CT, and the 30-mer dsDNA *gadd45* (Figure 7A–D). The data show that p53 DBD, p63 DBD and p73 DBD all bind to the latter specifically, forming protein−DNA complexes with similar mobility, though with different affinities. Using both agarose and native gels, we found that p73 DBD binds cooperatively to *gadd45* 30-mer dsDNA, which is similar to that of p53 DBD. Furthermore p73, p53 and p63 DBDs were found to bind to *Puma* and *bax* 30-mer dsDNAs in EMSA (data not shown), although the affinity was qualitatively different as judged by the intensity of the observed bands. Interestingly, the longer construct of p73 containing both the DBD plus TET domains (p73 CT) exhibited a very different pattern of binding relative to the corresponding p53 construct, containing p53 DBD plus TET domains (p53 CT) (Figure 7D). The data show that p53 CT binds *gadd45* forming a mixture of monomeric, dimeric and tetrameric complexes. However, p73 CT binds distinctly differently relative to p53 CT and appears to form a mixture of monomeric and tetrameric complexes (Figure 7D). It was reported previously that p53 DBD and a larger tetrameric construct, p53 CT, which included both the DBD and the C-terminal domains, bind to DNA in a

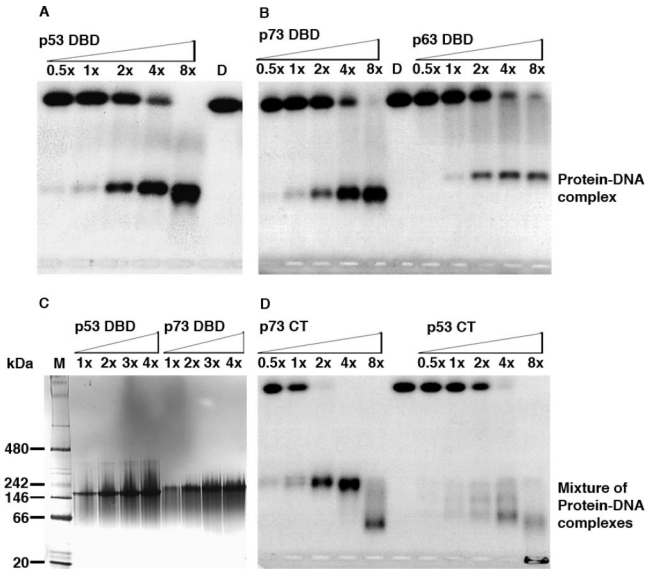

FIGURE 7: Electrophoretic mobility shift assays (EMSA) of the p53 family of proteins. Binding to *gadd45* dsDNA was used as a model system. Titration experiments were carried out for (A) p53 DBD, (B) p73 DBD and p63 DBD, and (D) p73 CT and p53 CT constructs at a DNA concentration of 1×10^{-8} M and increasing concentrations of protein (protein:DNA ratios are indicated above each lane, D indicates DNA alone). The analyses were performed using 0.7% agarose gels. (C) Titration experiments were carried out for p53 DBD and p73 DBD constructs as described above but using a DNA concentration of 15 μM and increasing protein concentrations (as indicated above each lane, M indicates the Native Mark marker). The analyses were performed on a 4–16% prepoured Native PAGE gel (Invitrogen).

cooperative manner (*39, 45*). Most recently Lokshin et al. reported that full-length p53 and p73 β display distinct requirements for sequence specific binding to DNA and concluded that zinc chelation by EDTA is significantly more detrimental to the ability of p73 β than p53 to bind DNA (*8*). The authors suggested that the loss of Zn is likely to have a greater effect on the conformation of p73 DBD than p53 DBD.

Modeling. In Figure 8 the electrostatic surfaces of the p53 dimer (A and B) and of the model-built p73 dimer (C and D) are shown. We report the surface views in Figure 8, with the DNA binding site perpendicular to the plane, and we also show the opposite face of this view (B and D). Although the main residues directly involved in the DNA binding site are conserved between p53 and p73, minor differences are found, as can be observed from Table 2, in which the residues buried upon dimerization are reported. The latter shows a quantification of the relative burial for these residues as obtained from our structural model. One of the differences emerging from our model regards the nature of electrostatic surface near the DNA binding site. p53 presents a larger electropositive surface when compared to p73. As can be seen in Figure 9 the phosphate groups are facing this surface when binding to p53, therefore this observation could serve as a possible explanation for the lower affinity of p73 for DNA when compared to p53. Another striking difference is found when comparing the opposite side of the electrostatic surface: p73 presents a diffused electronegative area, which is missing in p53 (Figure 8). This surface is due to aspartic acid and glutamic acid residues on the surface of p73 (ASP 120, GLU 128, GLU 185), which are absent or replaced by positively charged (ARG 110) or polar (GLN 167) residues in p53 according to the structure-based alignment (Figure 9A). This observation suggests that p53 and p73 could bind on this surface to two very different binding partners, one with a more acidic surface (p53) and one with a more basic surface (p73).

DISCUSSION

The work described here aims at investigating the thermal stability of the p73 protein and its ability to bind to DNA in order to shed further light on the structure and function of p73. Efforts were made to correlate the observations for p73 with p53 and p63 in order to better understand the intricate complexities and interplay within this family of proteins and their individual and collective functions in tumor suppression. A growing body of data highlights a plausible link between the intrinsic instability of p53 at physiological temperature and its function, which may play a unique role in regulating p53 cellular response. In the literature, information about p73 stability and how this might affect DNA binding activity and cellular response is vague and related mostly to the regulation of p73 turnover and the existence of transactivation-dependent and -independent mechanism(s) for p73 degradation (*46*). Moll et al. have reported that p73 differs from p53 in terms of cellular stability ($t_{1/2}$) with p53 being a short-lived protein whose stability is regulated by an autoregulatory MDM2 negative feedback loop (*10*). In sharp contrast to p53, p73 is not targeted for degradation by MDM2.

Dulloo and Sabapathy reported that the regions between amino acid residues 358–499 conferred destabilization, while the region between residues 248–358, conferred stability to p73 (*46*). The thermodynamic stability data and the apparent melting temperatures reported here for p73 DBD (104–333) and p73 CT (104–383) indicate that p73 DBD is thermodynamically more stable than p73 CT. This is in good agreement with the published data (*46*) related to the cellular stability of p73. Although the DSC and CD data presented here are qualitative, due to the irreversible thermal unfolding nature of the proteins, they still provide reliable information about the effects of temperature on stability. The apparent T_m data correlate with the observations from equilibrium chemical mediated denaturation studies. The in vivo stability of p73 proteins are contradictory because of the use of various overexpression systems. For example, the half-life of TAp73α has been reported as 2.25, 2, and 12 h, whereas the half-life of ΔNp73α has been reported to 0.5, 4, and 8 h (*47*). Accordingly, the apparent T_m data presented here might be useful in complementing and evaluating the current published data on p73 in vivo. The only quantitative biophysical data on p73 published so far concerns the isolated p73 tetramerization domain (p73 TET) (345–383) and the sterile alpha motif domain, SAM (487–554) (*6, 48*). The biochemical and structural data reported here provide novel information on the other key functional domains of the p73 protein (p73 DBD and p73 CT) and thus complement the knowledge about the isolated p73 TET domain and the p73 SAM domain. The data shown here demonstrate that p73 DBD exhibits enhanced thermal stability relative to the p53 DBD but not to the p63 DBD. The p73 DBD has been seen to be thermally more stable than the longer p73 CT.

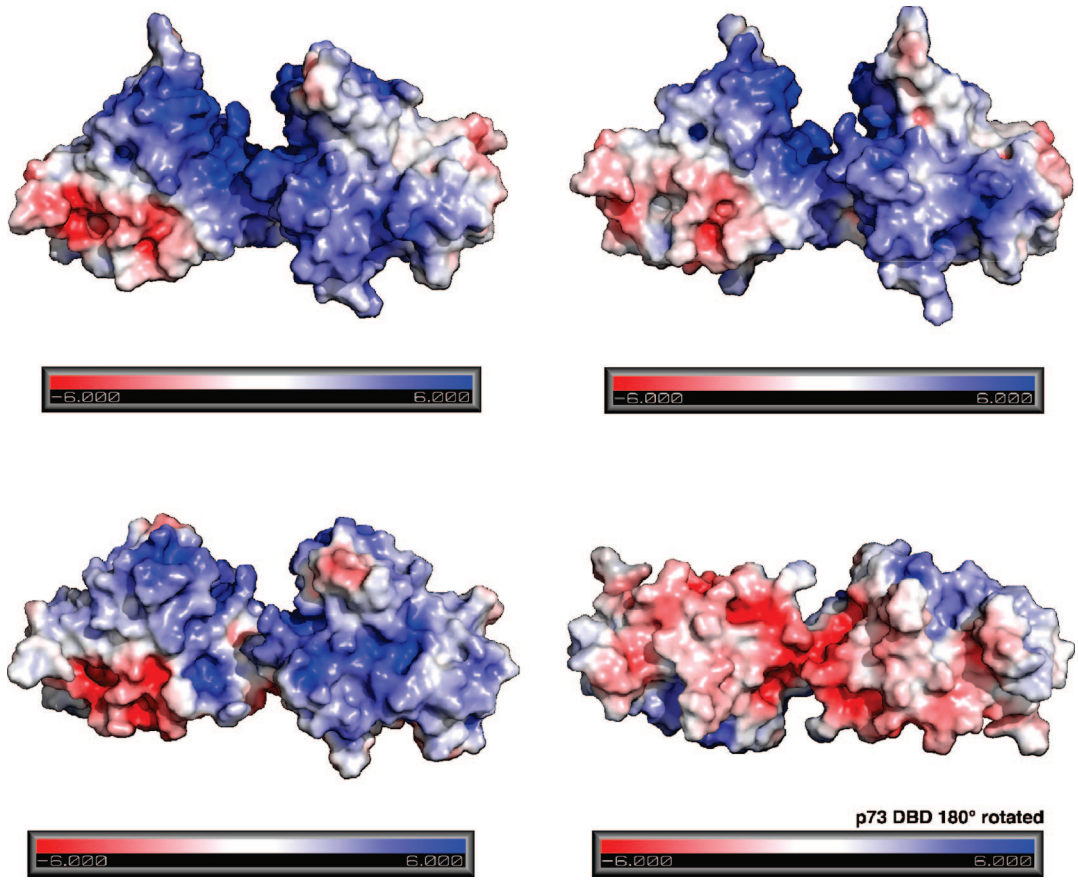

FIGURE 8: Structure-based homology modelling of the dimeric p73 DBD-DNA complex based on the p53 DBD−DNA complex. Comparison of the electrostatic potential of the p53 DBD based on 2aco dimer (A and B) and the predicted model of p73 DBD dimer (C and D). The potential ranges from the negative value –6*k*T (red) to the positive value +6*k*T (blue). For each complex, two views are presented: a front view along the DNA axis and the opposite face view obtained by rotation of 180°.

Our data and that of others have highlighted marked differences in the DNA binding between p73 and p53 as well as p63 and p53 for p53 promoter sequences (*8, 9, 38*). Importantly, whereas p63 (*38*) and p73 retain their ability to bind DNA at physiological temperature (P.N. and E.C. unpublished NMR data), p53 DBD shows greatly reduced binding (*38, 39*). The EMSA data presented here show that DBDs of all three proteins bind cooperatively to *gadd45* forming tetrameric protein−DNA complexes (Figure 7). Furthermore, it is known that p53 CT is able to bind to its promoter sequences in a cooperative manner (*49*). Our preliminary data for p73 CT indicate that p73 may have a different pattern of binding (Figure 7D). It has been suggested that specific residues in p53 (Lys 120, Ala 276, Arg 280), might account for stronger p53−DNA interactions. These residues are conserved in p73 and correspond to Lys 138, Ala 296, and Arg 300. Lokshin et al. have suggested that this could explain some of the similarities between p53 and p73β for DNA-binding sites in p53 REs (*8*). Observations by Klein et al. revealed that p63 DBD requires dimerization in order to be able to bind DNA (*38*). Others have speculated that because the key residues involved in dimerization of p53 DBD are basic residues (His 178 and Arg 181) and in p63 these are substituted by nonbasic residues (Asn 246, Leu 249), this could account for the differences in DNA binding (*50*). Furthermore, because p73 DBD has identical sequence with p63 in the H1 helix, the authors hypothesized that both p63 and p73 DBDs do not make the same dimer interactions with DNA as p53 DBD and hence this could account for the functional differences between the homologues. The greater similarities between p63 and p73 DBDs could be explained by the fact that p73 and p63 are more similar to each other in terms of sequence and possibly structure than to p53. The CD studies reported here, provided further support for the greater similarities between p73 and p63. The far-UV CD spectra of p63 DBD and p73 DBD are more similar to each other than either is to the corresponding CD of p53 DBD.

Monomeric p53 DBD is known to bind DNA specifically forming 4:1 protein: DNA complexes. However, the DNA binding of p53 CT (consisting of the DBD and the TET domains) is cooperative and has been reported recently to have a stoichiometry of two dimers binding per DNA molecule (*41, 49*). On the basis of our structural model of the p73 dimer complexed to DNA, we have identified some key differences occurring at the dimerization interface in the p73 model as compared to the p53 2AC0 crystal structure. In our structure-based alignment obtained by the superimposition of the p53 structure and the p73 model, we observed that the residues of the H1 p53 helix His 178 and Met 243 are not conserved in p73, and they correspond to residues Asn 196 and Val 263. We observed that Arg 181 in p53 corresponds to Arg 201 in p73, contradictory to the finding based on a sequence alignment that the same residue in p53 corresponds to Leu 199 (*8*). Our structural model depicts very elegantly the key differences between p73 and p53, especially around the dimer interface and the zinc atom. As shown in Figure 9D, the Met 243 of one subunit is protruding

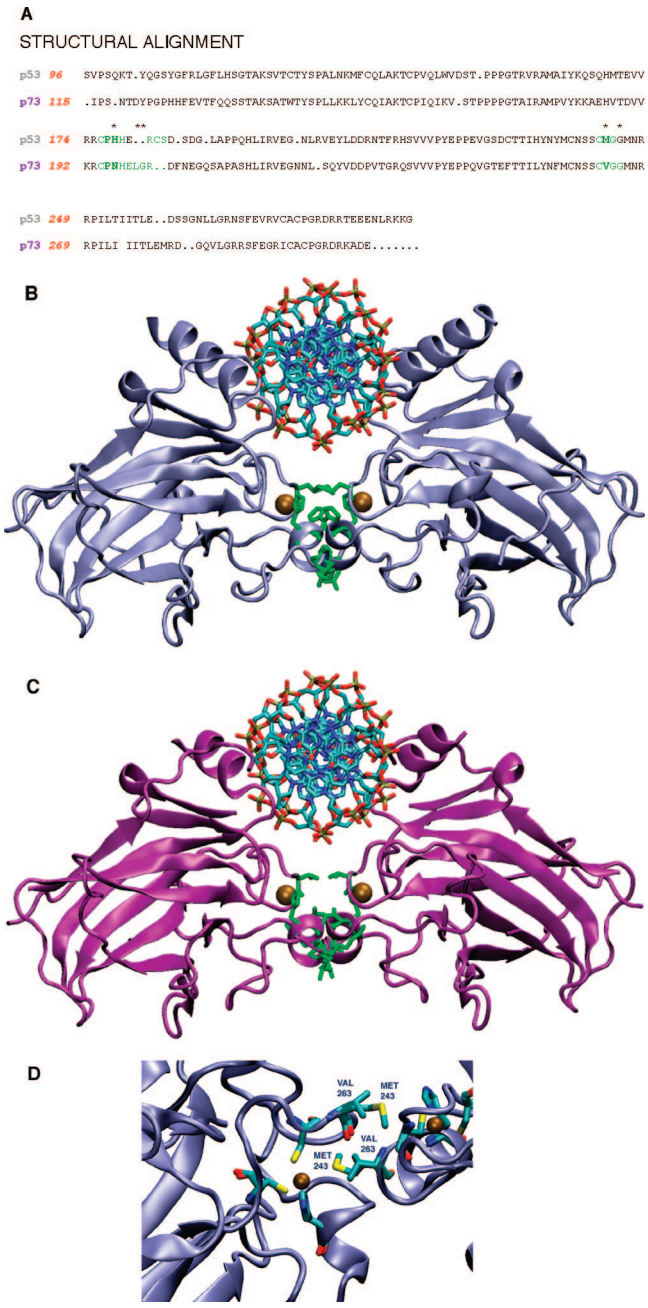

FIGURE 9: Sequence and structure comparison. (A) Structure-based sequence alignment of the dimerization interfaces of p53 DBD and the modelled p73 DBD. The residues at the dimerization interface are highlighted in green and the most significant differences between p53 and p73 residues are highlighted in bold. The star symbol (*) indicates the residues that differ in the two structures upon DNA binding. (B, C) Comparison of the p53 and p73 dimerization interface upon binding to DNA. The residues at the dimerization interfaces are shown in green liquorice; the Zn atom, gold; (B) p53 DBD, blue-grey; (C) p73 DBD, purple; the DNA molecule is shown at the top. (D) Close-up view of the dimerization interface showing the zinc cavity for the p73 model superimposed onto p53.

toward the other subunit, partly occluding the Zn cluster cavity. A substitution in this position with the smaller valine residue (Val 263 in p73) induces a larger cavity therefore resulting in a more tightly bound Zn atom for the p53 structure (Figure 9B) than for the p73 one (Figure 9C). In addition, we noted that Cys 182 and Ser 183 in p53 are absent in p73. Taken together, all these changes would cause the dimerization of p73 to be less stable, which could explain the observed difference in selectivity/specificity of p73 for p53 REs. These structural differences and the aforementioned difference in electrostatic surface could make p53 a better substrate for the interaction with DNA with respect to p73. Further investigation of the molecular mechanism of specificity and selectivity as well as of the structure of p73 with key cell cycle promoters is required to better understand the function of p73 and its role in p53 network and cancer.

ACKNOWLEDGMENT

We thank Assia Merabet for technical assistance, Dr. Peter Wong for providing clones for p73 and p63, Linda Chapman for help with EMSA, Prof. Sir Alan R. Fersht, FRS, for his support during the initial phase of this work, Prof. Daniela Rhodes, FRS, for critical discussions and feedback on the manuscript, and Prof. Brian Sutton for his invaluable advice during preparation of this manuscript.

REFERENCES

1. Laptenko, O., and Prives, C. (2006) Transcriptional regulation by p53: one protein, many possibilities. *Cell Death Differ. 13*, 951–961.
2. Murray-Zmijewski, F., Lane, D. P., and Bourdon, J. C. (2006) p53/p63/p73 isoforms: an orchestra of isoforms to harmonise cell differentiation and response to stress. *Cell Death Differ.*
3. Harms, K. L., and Chen, X. (2006) The functional domains in p53 family proteins exhibit both common and distinct properties. *Cell Death Differ. 13*, 890–897.
4. Cho, Y., Gorina, S., Jeffrey, P. D., and Pavletich, N. P. (1994) Crystal structure of a p53 tumor suppressor-DNA complex: understanding tumorigenic mutations. *Science 265*, 346–355.
5. Chi, S. W., Ayed, A., and Arrowsmith, C. H. (1999) Solution structure of a conserved C-terminal domain of p73 with structural homology to the SAM domain. *Embo J. 18*, 4438–4445.
6. Davison, T. S., Vagner, C., Kaghad, M., Ayed, A., Caput, D., and Arrowsmith, C. H. (1999) p73 and p63 are homotetramers capable of weak heterotypic interactions with each other but not with p53. *J. Biol. Chem. 274*, 18709–18714.
7. Lohrum, M. A., and Vousden, K. H. (2000) Regulation and function of the p53-related proteins: same family, different rules. *Trends Cell Biol. 10*, 197–202.
8. Lokshin, M., Li, Y., Gaiddon, C., and Prives, C. (2007) p53 and p73 display common and distinct requirements for sequence specific binding to DNA. *Nucleic Acids Res. 35*, 340–352.
9. Suh, E. K., Yang, A., Kettenbach, A., Bamberger, C., Michaelis, A. H., Zhu, Z., Elvin, J. A., Bronson, R. T., Crum, C. P., and McKeon, F. (2006) p63 protects the female germ line during meiotic arrest. *Nature 444*, 624–628.
10. Moll, U. M., and Slade, N. (2004) p63 and p73: roles in development and tumor formation. *Mol. Cancer Res. 2*, 371–386.
11. Yang, A., and McKeon, F. (2000) P63 and P73: P53 mimics, menaces and more. *Nat. Rev. Mol. Cell Biol. 1*, 199–207.
12. Lissy, N. A., Davis, P. K., Irwin, M., Kaelin, W. G., and Dowdy, S. F. (2000) A common E2F-1 and p73 pathway mediates cell death induced by TCR activation. *Nature 407*, 642–645.
13. Irwin, M., Marin, M. C., Phillips, A. C., Seelan, R. S., Smith, D. I., Liu, W., Flores, E. R., Tsai, K. Y., Jacks, T., Vousden, K. H., and Kaelin, W. G., Jr (2000) Role for the p53 homologue p73 in E2F-1-induced apoptosis. *Nature 407*, 645–648.
14. Flores, E. R., Tsai, K. Y., Crowley, D., Sengupta, S., Yang, A., McKeon, F., and Jacks, T. (2002) p63 and p73 are required for p53-dependent apoptosis in response to DNA damage. *Nature 416*, 560–564.
15. Flores, E. R., Sengupta, S., Miller, J. B., Newman, J. J., Bronson, R., Crowley, D., Yang, A., McKeon, F., and Jacks, T. (2005) Tumor predisposition in mice mutant for p63 and p73: evidence for broader tumor suppressor functions for the p53 family. *Cancer Cell 7*, 363–373.
16. Senoo, M., Manis, J. P., Alt, F. W., and McKeon, F. (2004) p63 and p73 are not required for the development and p53-dependent apoptosis of T cells. *Cancer Cell 6*, 85–89.
17. Arrowsmith, C. H. (1999) Structure and function in the p53 family. *Cell Death Differ. 6*, 1169–1173.

18. Wang, W., Kim, S. H., and El-Deiry, W. S. (2006) Small-molecule modulators of p53 family signalling and antitumor effects in p53-deficient human colon tumor xenografts. *Proc. Natl. Acad. Sci. U.S.A. 103*, 11003–11008.
19. Kitayner, M., Rozenberg, H., Kessler, N., Rabinovich, D., Shaulov, L., Haran, T. E., and Shakked, Z. (2006) Structural basis of DNA recognition by p53 tetramers. *Mol. Cell 22*, 741–753.
20. Bullock, A. N., Henckel, J., DeDecker, B. S., Johnson, C. M., Nikolova, P. V., Proctor, M. R., Lane, D. P., and Fersht, A. R. (1997) Thermodynamic stability of wild-type and mutant p53 core domain. *Proc. Natl. Acad. Sci. U.S.A. 94*, 14338–14342.
21. Miroux, B., and Walker, J. E. (1996) Over-production of proteins in Escherichia coli: mutant hosts that allow synthesis of some membrane proteins and globular proteins at high levels. *J. Mol. Biol. 260*, 289–298.
22. Gill, S. C., and von Hippel, P. H. (1989) Calculation of protein extinction coefficients from amino acid sequence data. *Anal. Biochem. 182*, 319–326.
23. Malik, K. M. (1997),London University.
24. Nikolova, P. V., Wong, K. B., DeDecker, B., Henckel, J., and Fersht, A. R. (2000) Mechanism of rescue of common p53 cancer mutations by second-site suppressor mutations. *Embo J. 19*, 370–378.
25. Nikolova, P. V., Henckel, J., Lane, D. P., and Fersht, A. R. (1998) Semirational design of active tumor suppressor p53 DNA binding domain with enhanced stability. *Proc. Natl. Acad. Sci. U.S.A. 95*, 14675–14680.
26. Pace, C. N. (1986) Determination and analysis of urea and guanidine hydrochloride denaturation curves. *Methods Enzymol. 131*, 266–280.
27. Jayaraman, L., Freulich, E., and Prives, C. (1997) Functional dissection of p53 tumor suppressor protein. *Methods Enzymol. 283*, 245–256.
28. Rost, B. (1999) Twilight zone of protein sequence alignments. *Protein Eng. 12*, 85–94.
29. Notredame, C., Higgins, D. G., and Heringa, J. (2000) T-Coffee: A novel method for fast and accurate multiple sequence alignment. *J. Mol. Biol. 302*, 205–217.
30. Marti-Renom, M. A., Stuart, A. C., Fiser, A., Sanchez, R., Melo, F., and Sali, A. (2000) Comparative protein structure modelling gene and genomes. *Annu. Rev. Biophys. Biomol. Struct. 29*, 291–325.
31. Berendsen, H. J. C., van der Spoel, D., and van Drunen, R. (1995) GROMACS: A message-passing molecular dynamics implementation. *Comput. Phys. Commun. 91*, 43–56.
32. Daura, X., Mark, A. E., and van Gunsteren, W. F. (1998) Parametrization of aliphatic CHn nited atoms of GROMOS96 force field. *J. Comput. Chem. 19*, 535–547.
33. Humphrey, W., Dalke, A., and Schulten, K. (1996) VMD: Visual molecular dynamics. *J. Mol. Graphics 14*, 33–38.
34. Kleinjung, J., and Fraternali, F. (2005) POPSCOMP: an automated interaction analysis of biomolecular complexes. *Nucleic Acids Res. 33*, W342–346.
35. Fraternali, F., and Cavallo, L. (2002) Parameter optimized surfaces (POPS): analysis of key interactions and conformational changes in the ribosome. *Nucleic Acids Res. 30*, 2950–2960.
36. DeLano, W. L. (2002) *The PyMOL Molecular Graphics System*, DeLano Scientific, SanCarlos, CA.
37. Baker, N. A., Sept, D., Joseph, S., Holst, M. J., and McCammon, J. A. (2001) Electrostatics of nanosystems: application to microtubules and the ribosome. *Proc. Natl. Acad. Sci. U.S.A. 98*, 10037–10041.
38. Klein, C., Georges, G., Kunkele, K. P., Huber, R., Engh, R. A., and Hansen, S. (2001) High thermostability and lack of cooperative DNA binding distinguish the p63 core domain from the homologous tumor suppressor p53. *J. Biol. Chem. 276*, 37390–37401.
39. Bell, S., Klein, C., Muller, L., Hansen, S., and Buchner, J. (2002) p53 contains large unstructured regions in its native state. *J. Mol. Biol. 322*, 917–927.
40. Nichols, N. M., and Matthews, K. S. (2001) Protein-DNA binding correlates with structural thermostability for the full-length human p53 protein. *Biochemistry 40*, 3847–3858.
41. Ang, H. C., Joerger, A. C., Mayer, S., and Fersht, A. R. (2006) Effects of common cancer mutations on stability and DNA binding of full-length p53 compared with isolated core domains. *J. Biol. Chem. 281*, 21934–21941.
42. Johnson, C. R., Morin, P. E., Arrowsmith, C. H., and Freire, E. (1995) Thermodynamic analysis of the structural stability of the tetrameric oligomerization domain of p53 tumor suppressor. *Biochemistry 34*, 5309–5316.
43. Mateu, M. G., Sanchez Del Pino, M. M., and Fersht, A. R. (1999) Mechanism of folding and assembly of a small tetrameric protein domain from tumor suppressor p53. *Nat. Struct. Biol. 6*, 191–198.
44. Weinberg, R. L., Veprintsev, D. B., Bycroft, M., and Fersht, A. R. (2005) Comparative binding of p53 to its promoter and DNA recognition elements. *J. Mol. Biol. 348*, 589–596.
45. Rippin, T. M., Freund, S. M., Veprintsev, D. B., and Fersht, A. R. (2002) Recognition of DNA by p53 core domain and location of intermolecular contacts of cooperative binding. *J. Mol. Biol. 319*, 351–358.
46. Dulloo, I., and Sabapathy, K. (2005) Transactivation-dependent and -independent regulation of p73 stability. *J. Biol. Chem. 280*, 28203–28214.
47. Sayan, A. E., Paradisi, A., Vojtesek, B., Knight, R. A., Melino, G., and Candi, E. (2005) New antibodies recognizing p73: comparison with commercial antibodies. *Biochem. Biophys. Res. Commun. 330*, 186–193.
48. Barrera, F. N., Garzon, M. T., Gomez, J., and Neira, J. L. (2002) Equilibrium unfolding of the C-terminal SAM domain of p73. *Biochemistry 41*, 5743–5753.
49. Veprintsev, D. B., Freund, S. M., Andreeva, A., Rutledge, S. E., Tidow, H., Canadillas, J. M., Blair, C. M., and Fersht, A. R. (2006) Core domain interactions in full-length p53 in solution. *Proc. Natl. Acad. Sci. U.S.A. 103*, 2115–2119.
50. Ho, W. C., Fitzgerald, M. X., and Marmorstein, R. (2006) Structure of the p53 core domain dimer bound to DNA. *J. Biol. Chem. 281*, 20494–20502.

BI7023207